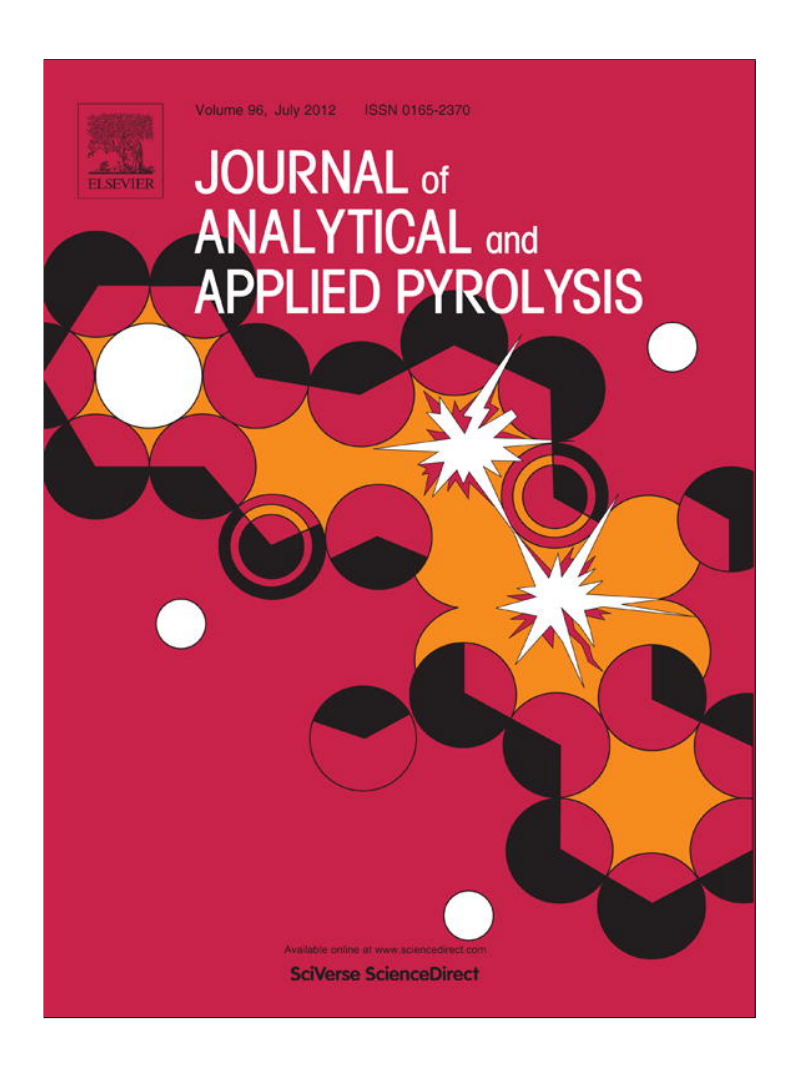
Provided for non-commercial research and education use. Not for reproduction, distribution or commercial use.



This article appeared in a journal published by Elsevier. The attached copy is furnished to the author for internal non-commercial research and education use, including for instruction at the authors institution and sharing with colleagues.

Other uses, including reproduction and distribution, or selling or licensing copies, or posting to personal, institutional or third party websites are prohibited.

In most cases authors are permitted to post their version of the article (e.g. in Word or Tex form) to their personal website or institutional repository. Authors requiring further information regarding Elsevier's archiving and manuscript policies are encouraged to visit:

http://www.elsevier.com/copyright

Author's personal copy

Journal of Analytical and Applied Pyrolysis 96 (2012) 63-68



Contents lists available at SciVerse ScienceDirect

Journal of Analytical and Applied Pyrolysis

journal homepage: www.elsevier.com/locate/jaap



Thermal degradation of magnetite nanoparticles with hydrophilic shell

Cristian-Dragos Varganici^a, Anamaria Durdureanu-Angheluta^a, Dan Rosu^{a,*}, Mariana Pinteala^a, Bogdan C. Simionescu^{a,b}

- a Centre of Advanced Research in Bionanoconjugates and Biopolymers, "Petru Poni" Institute of Macromolecular Chemistry, 41A Gr. Ghica-Voda Alley, 700487 Iasi, Romania
- ^b Department of Natural and Synthetic Polymers, "Gh. Asachi" Technical University of lasi, 73 B-dul Dimitrie Mangeron, 700050 lasi, Romania

ARTICLE INFO

Article history: Received 28 November 2011 Accepted 11 March 2012 Available online 17 March 2012

Keywords: Hybrid materials Thermogravimetric analysis Thermal degradation kinetics Evolved gas analysis

ABSTRACT

The aim of this study was the investigation of thermal degradation process at the interface of a core–shell type structure. Such hybrid compound was comprised of an inorganic core of magnetite nanoparticles and an organic shell consisting of 3-aminopropyltriethoxysilane. The thermal degradation has been studied by thermogravimetry in nitrogen atmosphere, up to 500 °C. The evolved gases analysis was performed using a coupling to a quadrupole mass spectrometer and a Fourier transform infrared spectrophotometer equipped with external modulus for gas analyses. Isoconversional kinetic study was conducted and a three stage thermal degradation mechanism was proposed.

© 2012 Elsevier B.V. All rights reserved.

1. Introduction

The research field of coated magnetite nanoparticles as substrate in bionanoconjugates has been expanding for more than three decades because of their potential as drug carriers for targeted drug delivery [1,2]. Therefore the establishment of accurate thermokinetical decomposition mechanisms plays an important role in the industrial processing of the future drug, especially for drugs in the form of oral tablets and capsules. Along with the appropriate pressing pressure, the temperature program must be rigorously selected in order to induce the specific cohesion forces and disintegration time once the tablet or capsule has reached the digestive tract [3]. This aspect is of greater importance especially in the field of controlled drug delivery or targeting. Other biomedical applications of magnetite nanoparticles are based on their magnetic properties. Such applications are: magnetic-force-based tissue engineering, magnetic enhanced transfection, magnetically induced hyperthermia and magnetically assisted gene therapy

The potential of drug delivery systems based on the use of magnetite nanoparticles as drug carriers brings three major advantages: (i) the ability to localize and target specific locations in the body; (ii) a seemingly reduced quantity of the drug needed to maintain a certain concentration in the proximity of the target; and (iii) the minimizing of side effects due to a reduction in the concentration of the drug at nontarget sites [6,7].

The thermooxidative degradation kinetics of solely precipitated magnetite particles were studied elsewhere and their decomposition into maghemite and hematite was reported [8–10].

The purpose of this paper is to obtain new knowledge and information about thermal stability of core–shell systems based on magnetite nanoparticles with polysiloxane coatings in inert atmosphere.

2. Experimental

2.1. Synthesis

The synthesis of 3-aminopropyltriethoxysilane covered magnetite nanoparticles M(III)APTES was submitted to a previous paper [11]. The existence of the core-shell structure as nanoparticles was proven by dynamic light scattering (DLS) technique and the diameters of the nanoparticles were found to be in the range 30–50 nm [11].

2.2. Measurements

The thermal degradation and evolved gas analyses of M(III)APTES were performed with a TGA-FTIR-MS system. The system was equipped with an apparatus of simultaneous TGA/DSC analyses STA 449F1 Jupiter model (Netzsch, Germany), FTIR spectrophotometer Vertex-70 model (Bruker, Germany), and mass spectrometer QMS 403C Aëolos model (Netzsch, Germany). The TG/DSC thermobalance was coupled online with FTIR spectrophotometer and mass spectrometer through two heated transfer lines. 9 mg were heated from 25 to 500 °C under nitrogen flow (flow

^{*} Corresponding author. Tel.: +40 232 217 454; fax: +40 232 211 299. E-mail addresses: drosu@icmpp.ro, dan_rosu50@yahoo.com (D. Rosu).

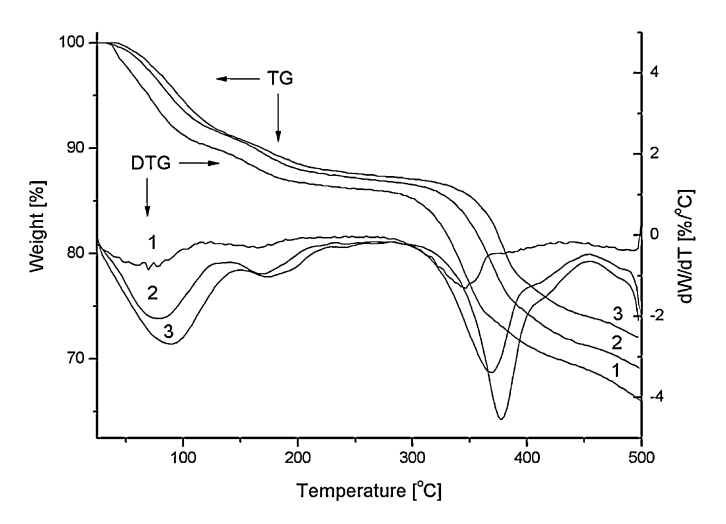


Fig. 1. TG and DTG curves recorded at different heating rates: (1) $5\,\rm K\,min^{-1}$; (2) $10\,\rm K\,min^{-1}$; (3) $20\,\rm K\,min^{-1}$.

rate 50 mL/min), in an open Al_2O_3 crucible and Al_2O_3 as reference material was used. Heating rates of 5, 10 and $20\,\mathrm{K\,min^{-1}}$ were used. The transfer line to FTIR spectrophotometer was made of polytetrafluorethylene, had an interior diameter of 1.5 mm and was heated at $190\,^{\circ}\mathrm{C}$. The spectra were acquired with a spectral resolution of $4\,\mathrm{cm^{-1}}$ on $400-4000\,\mathrm{cm^{-1}}$ range. The transfer line to MS spectrometer QMS $403\,\mathrm{C}$ is made of a quartz capillary with an internal diameter of $75\,\mu\mathrm{m}$ and was heated at $290\,^{\circ}\mathrm{C}$. The mass spectra were recorded under electron impact ionization energy of $70\,\mathrm{eV}$. Data were scanned in the range m/z=1-300, the measuring time for each cycle was $150\,\mathrm{s}$. The NIST Mass Spectral Database was used for the identification of ion fragments (m/z) in MS spectra. The kinetic analysis of thermogravimetric data was performed using the soft Netzsch Thermokinetic 3.

3. Results and discussion

3.1. Weight loss at different heating rates

Fig. 1 shows the TG and DTG curves of the sample M(III)APTES recorded at 5, 10 and $20\,\mathrm{K}\,\mathrm{min^{-1}}$ heating rates. The DTG curves indicate three stages of thermal decomposition.

Some characteristics extracted from TG and DTG curves are presented in Table 1 where $T_{\rm i}$ is the onset temperature of intense thermal degradation, $T_{\rm max}$ is the temperature that corresponds to the maximum rate of decomposition for each stage and $T_{\rm f}$ represents the final decomposition temperature. $T_{\rm i}$ is the intersection point of tangents to the two branches from the beginning of thermograms. $T_{\rm max}$ values were evaluated from the peaks of DTG curves. The final decomposition temperature $T_{\rm f}$ was determined by applying the same procedure as for $T_{\rm i}$ using the two branches from the end of thermograms. Table 1 also includes the mass loss rates corresponding to $T_{\rm max}$ values ($W_{\rm i}$) and the amount of residue remaining at the end of thermal degradation (500 °C).

It can be observed that the thermal degradation steps are shifted towards higher temperatures with the increase of the heating rate. This is due to temperature delay [12]. The quantity of the residue

that remained after thermal degradation varied between 66.11% and 72.18%, depending on the heating rate.

3.2. Kinetic analysis method

It was considered that thermal degradation of sample M(III)APTES follows the model reaction given in Eq. (1), where the solid material A(s) decomposes into solid residue R(s) and gases G(g).

$$A(s) \to R(s) + G(g)$$
 (1)

The kinetic parameters were evaluated from nonisothermal experiments. The conversion degree was calculated using Eq. (2), where m_0 , m_t and m_f represent the weights of the sample before degradation, at a time t, and after complete degradation.

$$\alpha = \frac{m_0 - m_t}{m_0 - m_f} \tag{2}$$

The kinetic model for Eq. (1) is Eq. (3), which is also the expression of the rate of thermal decomposition reaction, where α is the conversion degree of sample degradation, t is time (min), A is the pre-exponential factor (s⁻¹), E_a is the activation energy of thermal decomposition (kJ mol⁻¹), R is the gas constant (J mol⁻¹ K⁻¹), T is temperature (K) and $f(\alpha)$ is the conversion function.

$$\frac{d\alpha}{dt} = Ae^{-E_{\rm a}/RT}f(\alpha) \tag{3}$$

A new equation of the thermal degradation rate is obtained if one takes into account the rate of heating (Eq. (4)), $\beta = dT/dt$.

$$\frac{d\alpha}{dT} = \frac{A}{\beta} e^{-E_{a}/RT} f(\alpha) \tag{4}$$

After integration of Eq. (4) between the limits T_0 and T_p the integral function of conversion was obtained which was noted $G(\alpha)$ in Eq. (5).

$$G(\alpha) = \frac{A}{\beta} \int_{T_0}^{T_p} e^{-E_a/RT} dT = \int_0^{\alpha_p} \frac{d\alpha}{f(\alpha)}$$
 (5)

 T_0 is the initial temperature corresponding to α = 0 and T_p is the temperature corresponding to the peak from DTG curve, where $\alpha = \alpha_p$. The integral function of conversion depicts the mechanism of thermal degradation [13].

The kinetic parameters were evaluated using isoconversional Flynn–Wall–Ozawa method [14–16]. This method uses the thermograms shift to higher temperatures with the increase of heating rate. The relationship between kinetic parameters and the heating rate is given by Eq. (6).

ln
$$\beta = \ln\left(\frac{AE_a}{R}\right) - \ln G(\alpha) - 5.3305 - 1.052\frac{E_a}{RT}$$
 (6)

To calculate the kinetic parameters with Eq. (6) a first order reaction was assumed for $G(\alpha)$. For the same value of α , the plot of $\ln \beta$ as a function of 1/T is a straight line with the slope proportional with the activation energy.

By averaging of the three heating rates applied, $(\beta_{\rm m})$, Eq. (7) yields the values for $\ln A$, where $E_{\rm a}$ and α_j are known. If the presumption of first order kinetics proves valid, the plots of $\ln \beta$ versus 1/T must have the same slope. The different expressions of $G(\alpha)$

Table 1 Thermal decomposition characteristics of M(III)APTES.

Heating rate (°C min ⁻¹)	<i>T</i> _i (°C)	T _{max I} (°C)	W _I (%)	T _{max II} (°C)	W _{II} (%)	T _{max III} (°C)	W _{III} (%)	<i>T</i> _f (°C)	Residue mass (%)
5	37	70	9.3	155	12.8	346	26.9	371	66.1
10	43	76	8.2	150	13.4	355	28.7	454	69.1
20	47	89	8.6	174	13.7	456	26.9	456	72.2

C.-D. Varganici et al. / Journal of Analytical and Applied Pyrolysis 96 (2012) 63-68

Table 2Global kinetic parameters of thermal decomposition process of M(III)APTES resulted from Flynn–Wall–Ozawa method.

α	$E(kJ mol^{-1})$	$\log A(s^{-1})$
0.02	62	6.64
0.05	61	6.48
0.1	63	6.74
0.2	71	7.54
0.3	37	3.48
0.4	56	8.06
0.5	214	16.36
0.6	154	10.73
0.7	175	12.35
0.8	349	26.03

Table 3Kinetic parameters of the thermal decomposition stages of M(III)APTES.

Thermal decomposition stage	$E(kJ mol^{-1})$	$\log A(s^{-1})$	n
$A \rightarrow B$	60	6.83	2.99
$B \rightarrow C$	42	1.62	2.99
$C \rightarrow D$	158	11.23	2.06

which are specific to the thermal degradation mechanisms of polymers can be found in the literature [13].

$$\ln A = \ln[-\ln(1-\alpha)] - \ln\frac{E_a}{R} + \ln\beta_m - \ln p(z)$$
 (7)

The non-isothermal data extracted from the thermograms were processed with the software Netzsch Thermokinetics 3. The values of the kinetic parameters obtained by Flynn–Wall–Ozawa method for values of α ranging between 0.05 and 0.8 are given in Table 2.

It can be observed from Table 2 that the activation energy value varies with conversion suggesting the existence of at least three successive stages of decomposition. The first stage of thermal decomposition occurs at low conversion degrees (α between 0.02 and 0.2) when the activation energy gradually increases from 60 to 71 kJ mol⁻¹. Initial slight decrease of activation energy could associate with breaking initiation of some weak linkages and the relative rapid increase of E_a in the range 0.05 < α < 0.2 correspond to the consummation of the weak linkages [17]. The second stage

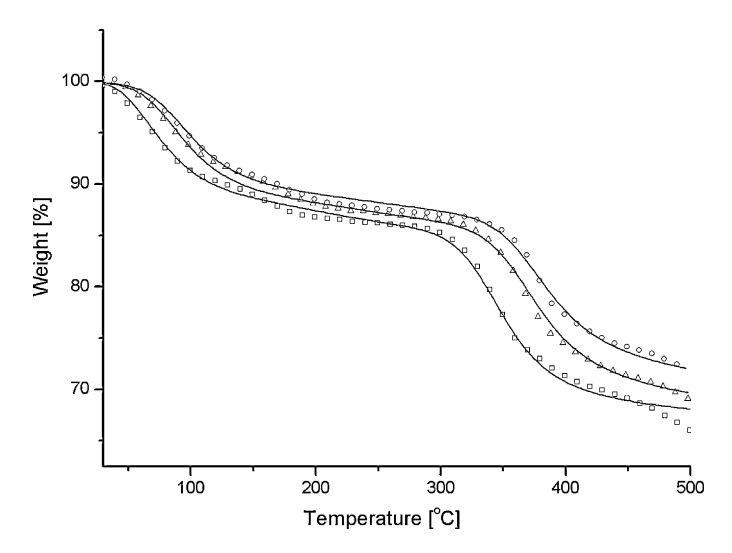


Fig. 2. Comparison of experimental TGA curves with the ones calculated from kinetic data: (\square) 5 K min $^{-1}$; (\triangle) 10 K min $^{-1}$; (\bigcirc) 20 K min $^{-1}$; (-) curves calculated from kinetic data.

of thermal decomposition occurs in the range $0.3 < \alpha < 0.5$. In this range the activation energy increases from $37 \, \text{kJ} \, \text{mol}^{-1}$ up to $214 \, \text{kJ} \, \text{mol}^{-1}$. The third stage of thermal decomposition occurs in the range $0.6 < \alpha < 0.8$ when the activation energy increases from $154 \, \text{kJ} \, \text{mol}^{-1}$ up to $349 \, \text{kJ} \, \text{mol}^{-1}$. In all the three stages of thermal decomposition the values of the kinetic parameters increase with the conversion degree, thus suggesting that the sample degrades in a complex pattern [18].

Multivariant non-linear regression method was performed to determine reaction model for the three heating rates and to find the real form of the conversion function [18]. A model of thermal decomposition in three successive stages (Eq. (8)) was proposed. In Eq. (8) *D* represents the thermostabile residue and *B* and *C* are solid intermediates.

$$A \xrightarrow{1} B \xrightarrow{2} C \xrightarrow{3} D$$
 (8)

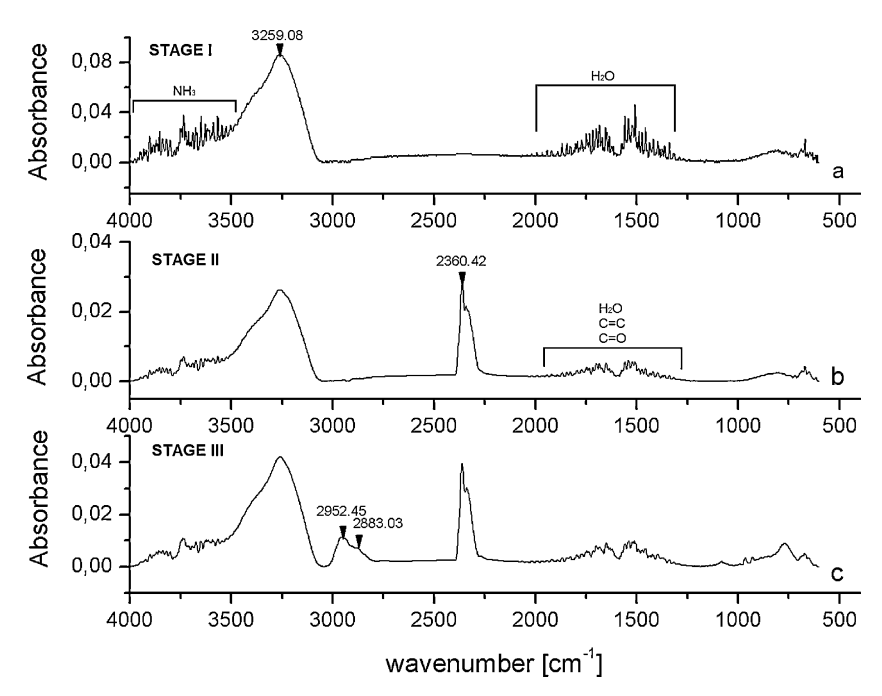


Fig. 3. FTIR spectra of evolved gases during: (a) the first, (b) the second and (c) the third thermal decomposition stage.

C.-D. Varganici et al. / Journal of Analytical and Applied Pyrolysis 96 (2012) 63-68

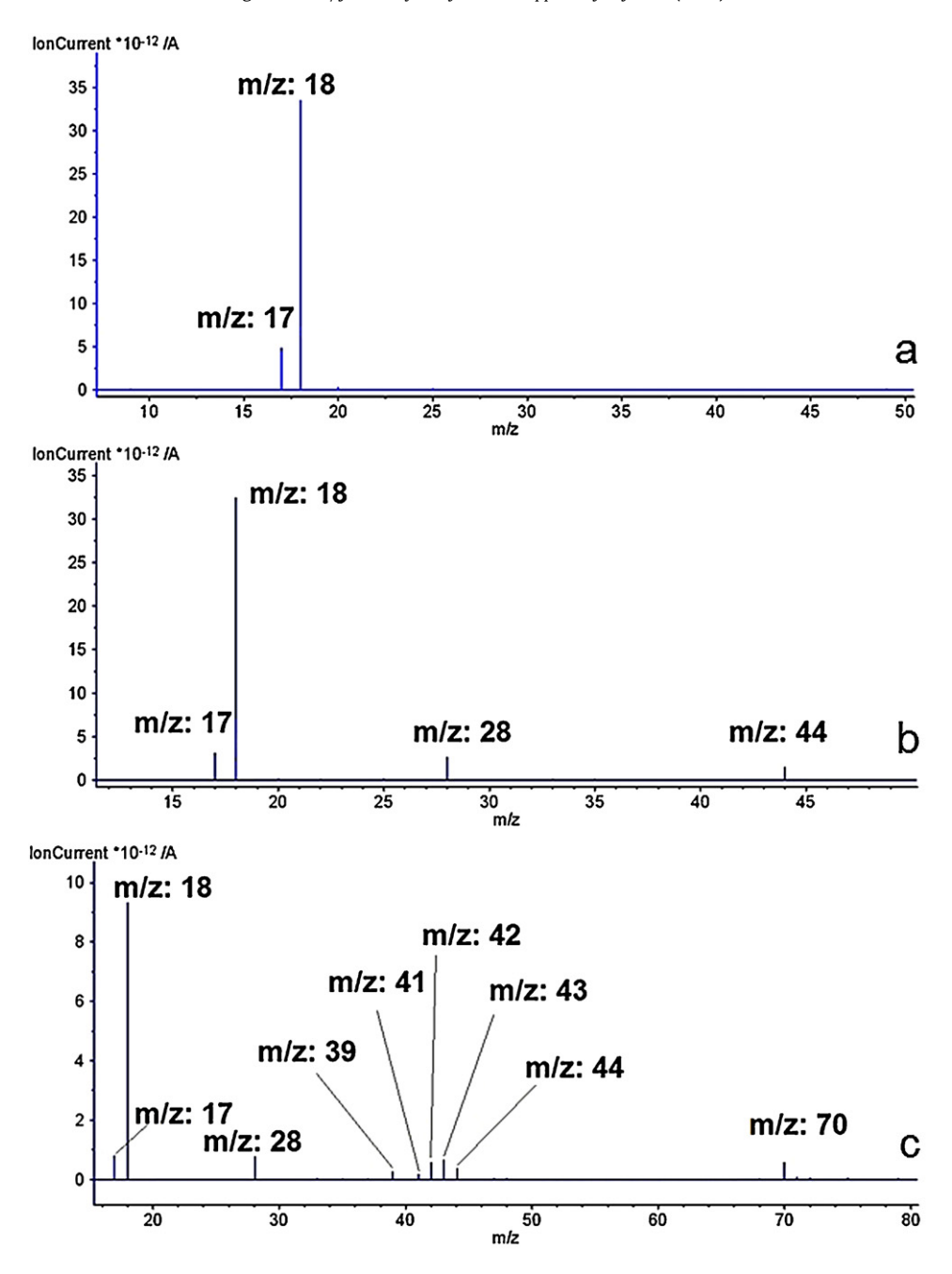


Fig. 4. MS spectra of evolved gases during: (a) the first, (b) the second and (c) the third thermal decomposition stage.

After testing of 16 reaction types the best results were obtained with n order reaction as described by Eq. (9), where n is the reaction order [19].

$$f(a) = (1 - \alpha)^n \tag{9}$$

The kinetic data obtained by the multivariant non-linear regression method are presented in Table 3.

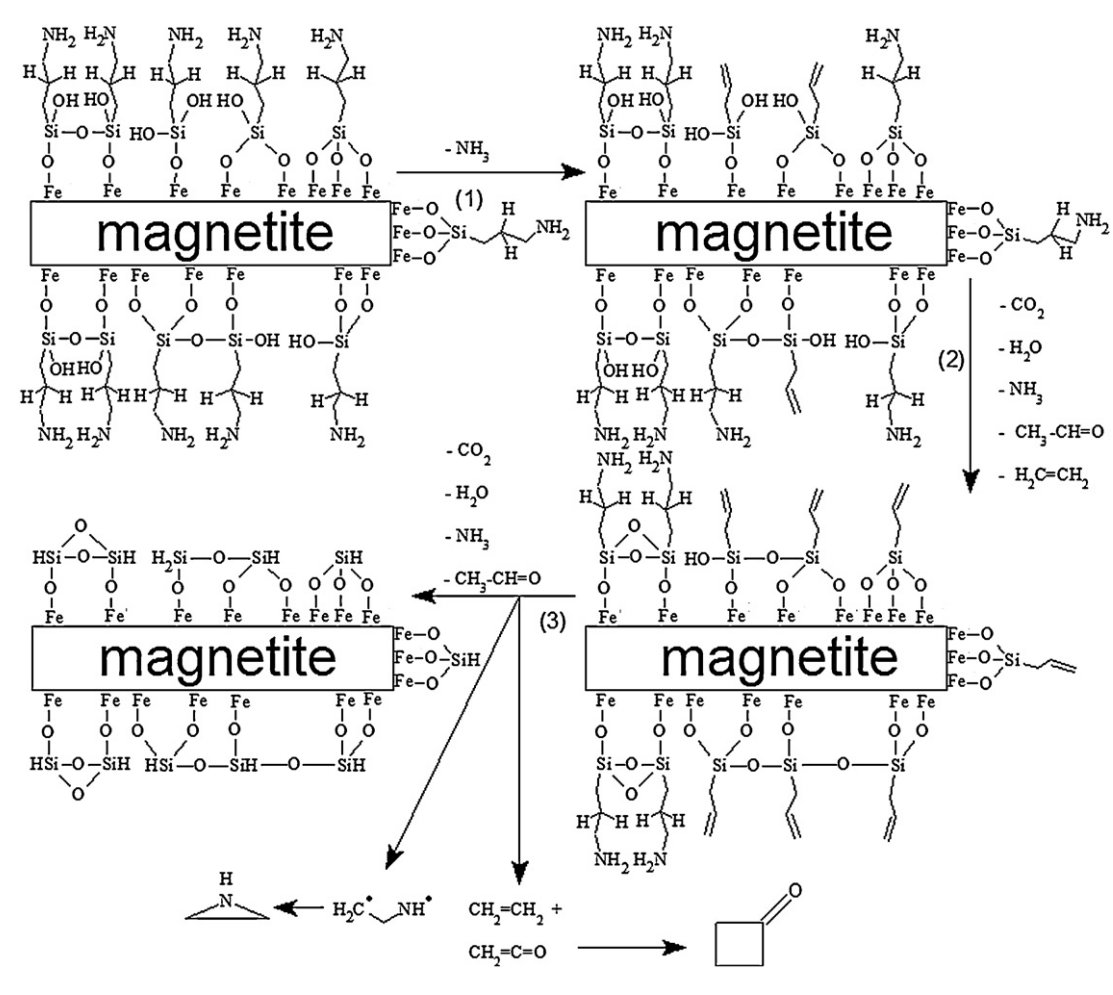
The experimental TGA curves were compared with those simulated by the software, using data presented in Table 3.

Fig. 2 shows the comparison of experimental data with the calculated data. The correlation coefficient yielded a value of 0.9987, thus proving the validity of M(III)APTES thermal decomposition model in three successive stages.

3.3. FTIR analysis of the evolved gases

Fig. 3 shows the FTIR spectra of the evolved gaseous products from all three stages of thermal decomposition. The broad peak at 3259 cm⁻¹ and the region from 1300 cm⁻¹ to around 2000 cm⁻¹ were attributed to the loss of physically absorbed water in the first stage of thermal decomposition (Fig. 3a) and that of covalently bonded water in the other two stages (Fig. 3b and c). The absorption bands in the range 3500–4000 cm⁻¹ correspond to N–H bond stretching vibration in ammonia [20]. It should be mentioned that the losses of water and ammonia were more intense in the first stage of thermal degradation (Fig. 3a). This aspect was correlated with a mass loss between 8.24 and 9.27% on the TGA curves, maybe because of the hydrophilicity of the nanoparticles. The peak at 2360 cm⁻¹ (Fig. 3b and c) corresponds to the loss of carbon

C.-D. Varganici et al. / Journal of Analytical and Applied Pyrolysis 96 (2012) 63-68



 $\textbf{Fig. 5.} \ \ \textbf{Schematic of the proposed thermal degradation mechanism of M(III)} \textbf{APTES.}$

dioxide. In the third stage of thermal decomposition (Fig. 3c) two peaks were observed at 2952 cm⁻¹ and 2883 cm⁻¹ corresponding to CH bond stretching in methyl group and methylene group from aliphatic amine [20,21]. The peaks from 1800 to 1300 cm⁻¹ region represent vibrations of C=O and C=C bands overlapping with those from water loss.

3.4. MS analysis of the evolved gases

Interpretations of mass spectra were made in correlation with FTIR spectra and NIST Mass Spectral Database. The MS analysis confirmed the presence of water and ammonia in the gaseous mixture resulted in all stages of thermal decomposition, which was proved by the fragments m/z=18 and/or 17. The m/z values of 28 and 44 in the second (Fig. 4b) and third (Fig. 4c) stage of thermal degradation represent ethene and both carbon dioxide and acetaldehyde. The last stage of thermal decomposition exhibits all the above mentioned m/z values. The m/z signals of 41 and 39 indicate the formation of ethylamine radicals, m/z=43 corresponds to the cyclic structure of aziridine and m/z=70 represents cyclobutanone. The m/z signal at 42 was attributed to ketene structure.

3.5. Thermal decomposition mechanism

The proposed thermal degradation mechanism of M(III)APTES is presented in Fig. 5. The loss of ammonia occurs continuously through random scission of the $C-NH_2$ bond.

Double bonds were formed due to the extraction of hydrogen atoms from the methylene group located in second position in propylamine chain.

In the second and third stages of thermal decomposition, the sample loses chemical bonded water by statistical scission of Si—OH bond. The second stage leads to the formation of cyclic structures based on Si—O—Si bonds. As electron acceptors, oxygen atoms thermally stabilize the cyclic Si—O—Si structures [22]. In addition, the low molecular weight cyclic siloxanes have an entropically higher stability than that of their high molecular weight open chain counterparts at degradation temperatures [23,24]. Because of random scission of hydrocarbon radicals, carbon dioxide is formed. Formation of ethene and acetaldehyde occurs also.

In the third stage of thermal decomposition, mass spectra and FTIR spectra indicate intense scissions of Si—C bonds generating a higher concentration of propylamine radicals which form aziridine cycle via cyclization reaction. According to the literature, the ethyleneimine (aziridine cycle) diluted with argon proceeds to give a mixture of unidentified compounds only at temperatures in the range of $400-500\,^{\circ}$ C [25]. These compounds correspond to the m/z values of 41 and 39 (Fig. 4c). The m/z value of 42 corresponds to ketene, which is known to be generally very reactive at high temperature and participates in various cycloaddition reactions [26].

Cyclobutanone structure (m/z = 70) is present via [2+2] cycloaddition between ketene and ethene [27]. The temperature range 360–400 °C is characteristic for obtaining of cyclobutanone via cycloaddition [28]. The high quantity of remained residue after complete degradation consists mainly of the highly thermostable magnetite and the mostly Si—O—Si network bonded at the interface through Fe—O—Si bonds.

4. Conclusions

The simultaneous TG-FTIR-MS analyses indicate that the sample M(III)APTES presented three stages of thermal decomposition in inert atmosphere. The kinetic parameters and the conversion function of each stage of decomposition were determined. A conversion function of n order was found. The software yielded a good correlation between experimental data and data calculated with the established kinetic model. A mechanism of thermal degradation of M(III)APTES was proposed based on FTIR and MS spectra of evolved gases mixture during thermal degradation. It was observed that thermal decomposition of M(III)APTES began with water and ammonia elimination throughout the whole degradation process, and the formation of C=C and C=O bonds. The second and third thermal decomposition stages presented losses of covalently bonded water, carbon dioxide and carbonyl and olefin products. These products underwent [2+2] cycloadditions with cyclobutanone formation in the third stage of thermal decomposition. Aziridine cycle was formed also in the third stage of thermal decomposition via cyclization

The obtained results may be applied in processing of the future tablet or pill, because, in both granulation, if needed, and compression processes, humidity and temperature values at the magnetite-ATPES interface must be well known and controlled within established parameters range. Thermal stability must also be known for industrial processing.

Acknowledgement

This research was financially supported by a grant of the Romanian National Authority for Scientific Research, CNCS – UEFISCDI, project number PN-II-ID-PCE-2011-3-0187.

References

- S.C. McBain, H.H.P. Yiu, J. Dobson, Magnetic nanoparticles for gene and drug delivery, Int. J. Nanomed. 3 (2008) 169–180.
- [2] M. Shinkai, Functional magnetic particles for medical application, J. Biosci. Bioeng. 94 (2002) 606–613.
- [3] S.E. Leucuta, Industrial Technological Pharmaceutics, Dacia, Iasi, 2008.
- [4] J. Corchero, A. Villaverde, Biomedical applications of distally controlled magnetic nanoparticles, Trends Biotechnol. 27 (2009) 468–476.

- [5] J. Chomoucka, J. Drbohlavova, D. Huska, V. Adam, R. Kizek, J. Hubalek, Magnetic nanoparticles and targeted drug delivering, Pharmacol. Res. 62 (2010) 144–149.
- [6] M. Arruebo, R. Fernandez-Pacheco, M.R. Ibarra, J. Santamaria, Magnetic nanoparticles for drug delivery, Nano Today 2 (2007) 22–32.
- [7] S. Mornet, S. Vasseur, F. Grasset, P. Veverka, G. Goglio, A. Demourgues, et al., Magnetic nanoparticle design for medical applications, in: Meeting of the European Materials Research Society, Pergamon-Elsevier Science Ltd, Strasbourg, 2005, pp. 237–247.
- [8] K. Przepiera, Podstawy otrzymywania strącanych pigmentów żelazowych, Thesis, Technical University of Szczecin, Szczecin, 1995.
- [9] A. Przepiera, K. Przepiera, M. Wiśniewski, W. Dabrowski, Enthalpy of solution and effect of temperature on activity coefficients in MSO₄-H₂SO₄-H₂O system, J. Therm. Anal. 40 (1993) 1139–1143.
- [10] A. Przepiera, K. Przepiera, M. Wiśniewski, M. Jabłoński, Determination of phase transformation of precipitated iron oxides in temperature range 298–1073 K, Mater. Sci. Forum 133–136 (1993) 599–602.
- [11] A. Durdureanu-Angheluta, A. Dascalu, A. Fifere, A. Coroaba, L. Pricop, H. Chiriac, V. Tura, M. Pinteala, B.C. Simionescu, Progress in the synthesis and characterization of magnetite nanoparticles with amino groups on the surface, J. Magn. Magn. Mater. 324 (2012) 1679–1689.
- [12] D. Rosu, N. Tudorachi, L. Rosu, Investigations on the thermal stability of a MDI based polyurethane elastomer, J. Anal. Appl. Pyrol. 89 (2010) 152–158.
- [13] M. Villanueva, J.L. Martin-Iglesias, J.A. Rodriguez-Anon, J. Proupin-Castineiras, Thermal study of an epoxy system DGEBA (n = 0) MXDA modified with POSS, J. Therm. Anal. Calorim. 96 (2009) 575–582.
- [14] J. Opfermann, E. Kaisersberger, An advantageous variant of the Ozawa-Flynn-Wall analysis, Thermochim. Acta 203 (1992) 167–175.
- [15] T. Ozawa, A new method of analysing thermogravimetric data, Bull. Chem. Soc. Jpn. 38 (1965) 1881–1886.
- [16] J.H. Flynn, L.A. Wall, A quick, direct method for the determination of activation energy from thermogravimetric data, J. Polym. Sci. Part B: Polym. Lett. 4 (1966) 323–328
- [17] P. Budrugeac, Theory and practice in the thermoanalytical kinetics of complex process: application for the isothermal and non-isothermal thermal degradation of HDPE, Thermochim. Acta 500 (2010) 30–37.
- [18] J. Opferman, Kinetic analysis using multivariate non-linear regression, J. Therm. Anal. Calorim. 60 (2000) 641–658.
- [19] A.K. Galwey, M.E. Brown, Kinetic background to thermal analysis and calorimetry, in: M.E. Brown (Ed.), Handbook of Thermal Analysis and Calorimetry, Elsevier Science, Amsterdam, 1998, pp. 179–181.
- [20] K. Can, M. Ozmen, M. Ersoz, Immobilization of albumin on aminosilane modified superparamagnetic magnetite nanoparticles and its characterization, Colloids Surf. B: Biointerfaces 71 (2009) 154–159.
- [21] R.M. Silverstein, F.X. Webster, D.J. Kiemle, Spectrometric Identification of Organic Compounds, Wiley, New York, 2005.
- [22] W. Noll, Chemie und technologie der silicon, Verlag Chemie GMBH, Weinheim-Bergstr., 1968, p. 278.
- [23] P.R. Dvornic, Thermal properties of polysiloxanes, in: R.G. Jones, W. Ando, J. Chojnowski (Eds.), Silicon Containing Polymers, Kluwer Academic Publishers, Dordrecht, 2000, pp. 185–212.
- [24] P.R. Dvornic, R.W. Lenz, High Temperature Siloxane Elastomers, Huthig and Wepf, Basel, 1990.
- [25] S.V. Zotova, G.V. Loza, M.Y. Lukina, Thermal transformations of ethylenimines, Bull. Acad. Sci. USSR 16 (1967) 415–417.
- [26] R.W. Holder, Ketene cycloadditions, J. Chem. Educ. 53 (1976) 81–85.
- [27] L.A. Burke, Theoretical study of (2+2) cycloadditions. Ketene with ethylene, J. Org. Chem. 50 (1985) 3149–3155.
- [28] M.N. Das, F. Kern, T.D. Coyle, W.D. Walters, The thermal decomposition of cyclobutanone, J. Am. Chem. Soc. 76 (1954) 6271–6274.